Optics Letters

# Reconstruction design method of an aspherical recording optical system for the varied line-space grating

Xinyu Wang,[1,2] Yanxiu Jiang,[1] Zhongming Zheng,[1] Wei Wang,[1] Zhendong Chi,[1] and Wenhao Li[1,*]

[1]Changchun Institute of Optics, Fine Mechanics and Physics, Chinese Academy of Sciences, Changchun, Jilin, 130033, China
[2]University of Chinese Academy of Sciences, Beijing, 100049, China
*Corresponding author: liwh@ciomp.ac.cn

Received 5 July 2022; revised 10 August 2022; accepted 11 August 2022; posted 11 August 2022; published 26 August 2022

**A reconstruction design method for an aspherical recording system for varied line-space gratings is introduced. This method converts the recording system design from achieving specific groove distribution coefficients within the expansion model into reconstruction of the auxiliary mirror surface via the ray-tracing method. The effects of higher-order expansion terms in the expansion model are investigated and more accurate design of the varied line-space grating recording structure is achieved. By varying the surface reconstruction target, this method can be used to design aspherical recording structures with any auxiliary mirror surface shapes.** © 

https://doi.org/10.1364/OL.469523

The varied line-space (VLS) grating, in which the line-spacing varies throughout the grating surface, has been studied for decades. This type of grating is used widely in spectrometers because of its focusing and aberration-correcting capabilities [1–3]. A high-resolution spectrometer comprising only a single component can be achieved with use of the VLS grating. Uncontrollable stray light and energy loss due to additional optical elements are effectively avoided. Spectrometers with a VLS grating have a wide range of applications that include synchrotron radiation light sources and space-to-ground spectral imaging-based remote sensing, among other fields [4–10].

At present, the main manufacturing method for the VLS grating is interference lithography based on use of two nonplanar coherent beams. By varying the generating optical paths of these recording beams, a VLS grating recording structure can be realized that can generate specific groove distributions. Typical recording structures include double spherical wavefront recording structures, single or double aspherical wavefront recording structures with additional auxiliary mirrors, and several other specialized recording structures [11–15]. The mainstream method used to design the VLS grating recording structure involves analysis of the expansion coefficients within different recording structures based on optical path function theory and obtaining an expansion solution with a suitable optimization algorithm [11,14,15]. Because the higher-order terms included in the expansion model are ignored, the results obtained by this method always contain an inherent residual error that affects the theoretical accuracy of the designed VLS grating. To achieve different design goals, auxiliary mirrors with different surface types are often used within the recording structure to achieve different levels of wavefront control. For these different auxiliary mirror types, traditional methods require corresponding expansion models to be constructed, while some complex surface mirrors, e.g., freeform mirrors [12,16], further increase the complexity of the expansion models and the design difficulty.

In this Letter, we propose a reconstruction design method for the aspherical recording systems used for VLS gratings. The complete setup of the proposed method transforms the design of the recording structure for the VLS grating from one based on forward achievement of the target groove distribution to one based on reconstruction of the auxiliary mirror surface using the ray-tracing method, thus avoiding the higher-order expansion error involved in the expansion groove method. By varying the solution type of the target mirror surface, this method can be applied to optimal design of aspherical recording structures with different auxiliary mirror types for VLS gratings. A comparison of the design results obtained when using the traditional method and the proposed reconstruction method is presented for a planar VLS grating that shows that the reconstruction method can realize more accurate results for the recording systems. A design result obtained when using a freeform mirror rather than a spherical mirror shows that the method can be applied to the design of various aspherical recording structure types. The numerous design degrees of freedom for the freeform mirror are helpful in allowing complex groove distributions to be achieved. In addition, the groove distribution of the VLS grating is always allowed to have a specified tolerance. In our design method, the groove distribution tolerance also forms part of the design optimization. This additional design tolerance effectively reduces the design process difficulty.

The reconstruction design method described above is used to solve for the parameters of the recording system for a VLS grating in which an auxiliary mirror is added to one beam. The design parameters include recording structure parameters ($L_{RC}$, $L_{RQ}$, $L_{RD}$, $\theta_C$, $\theta_Q$, $\theta_D$) and the surface type of the auxiliary mirror.

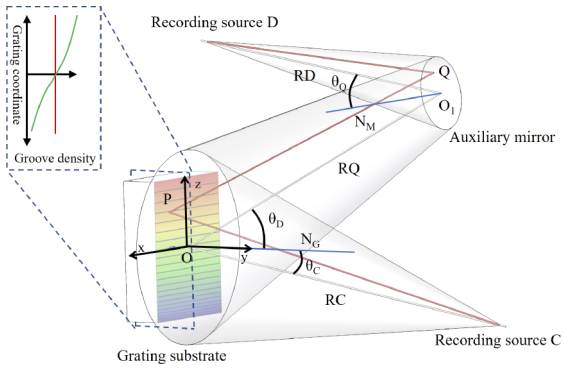


**Fig. 1.** Illustration of recording system for a holographic VLS grating with an auxiliary mirror.

Figure 1 shows an illustration of the complete recording system. Among the parameters shown in Fig. 1, $O_1$ and $O$ are the center points of the auxiliary mirror and the grating substrate, respectively, and point $P$ is the point of intersection of the grating substrate and the light ray reflected from point $Q$ on the auxiliary mirror. Coherent beams from the two laser sources at $C$ and $D$ will generate the required groove on the grating substrate. According to optical path theory [11], the groove function $n$ of point $P$ can be represented by the relative optical path difference between points $P$ and $O$. Assuming that the recording wavelength here is $\lambda$, the groove function can be represented as

$$n = \frac{1}{\lambda}\left[L_{CP} - L_{DQP} - \left(L_{CO} - L_{DO_1O}\right)\right] \approx \sum_{i+j>0}^{i+j\le 4} n_{ij} x_P^i z_P^j. \quad (1)$$

Because the groove function $n$ is relatively complex, it is always converted into a fourth-order polynomial form of the sagittal and meridional coordinates of point $P$ on the grating surface, where $n_{ij}$ stands for the expansion parameter to the basement $x^i z^j$ in the groove function $n$. Additionally, the coordinates of reflection point $Q$ on the auxiliary mirror will also be expanded into a polynomial form of the coordinates of point $P$. By then deriving the partial derivative of Eq. (1), expressions can be obtained for the meridional and sagittal components of the groove density:

$$\begin{aligned}\lambda\frac{\partial n}{\partial x_P} =& \alpha_{CP} + \beta_{CP}\frac{\partial y_P}{\partial x_P} - \alpha_{DQ}\frac{\partial x_Q}{\partial x_P} - \beta_{DQ}\frac{\partial y_Q}{\partial x_Q}\frac{\partial x_Q}{\partial x_P} - \\ & \beta_{DQ}\frac{\partial y_Q}{\partial z_Q}\frac{\partial z_Q}{\partial x_P} - \gamma_{DQ}\frac{\partial z_Q}{\partial x_P} - \alpha_{PQ}\frac{\partial x_Q}{\partial x_P} - \beta_{PQ}\frac{\partial y_Q}{\partial x_Q}\frac{\partial x_Q}{\partial x_P} \\ & + \alpha_{PQ} - \beta_{PQ}\frac{\partial y_Q}{\partial z_Q}\frac{\partial z_Q}{\partial x_P} + \beta_{PQ}\frac{\partial y_P}{\partial x_P} - \gamma_{PQ}\frac{\partial z_Q}{\partial x_P},\end{aligned} \quad (2)$$

$$\begin{aligned}\lambda\frac{\partial n}{\partial z_P} =& \gamma_{CP} + \beta_{CP}\frac{\partial y_P}{\partial z_P} - \alpha_{DQ}\frac{\partial x_Q}{\partial z_P} - \beta_{DQ}\frac{\partial y_Q}{\partial x_Q}\frac{\partial x_Q}{\partial z_P} \\ & - \beta_{DQ}\frac{\partial y_Q}{\partial z_Q}\frac{\partial z_Q}{\partial z_P} - \gamma_{DQ}\frac{\partial z_Q}{\partial z_P} - \alpha_{PQ}\frac{\partial x_Q}{\partial z_P} - \beta_{PQ}\frac{\partial y_Q}{\partial x_Q}\frac{\partial x_Q}{\partial z_P} \\ & - \beta_{PQ}\frac{\partial y_Q}{\partial z_Q}\frac{\partial z_Q}{\partial z_P} + \beta_{PQ}\frac{\partial y_P}{\partial z_P} - \gamma_{PQ}\frac{\partial z_Q}{\partial z_P} + \gamma_{PQ},\end{aligned} \quad (3)$$

where $\alpha$, $\beta$, and $\gamma$ represent the $x$, $y$, and $z$ components of the directional vector for the corresponding light ray. Here, $x$, $y$, and $z$ represent the coordinates of the corresponding point. At the same time, for the optical path of the system shown in Fig. 1, the partial derivative of the optical path $L_{DQP}$ with respect to the coordinates of point $Q$ should have a value of zero according to Fermat's principle, i.e.,

$$0 = \frac{\partial L_{DQP}}{\partial x_Q} = \alpha_{DQ} + \beta_{DQ}\frac{\partial y_Q}{\partial x_Q} + \alpha_{PQ} + \beta_{PQ}\frac{\partial y_Q}{\partial x_Q}, \quad (4)$$

$$0 = \frac{\partial L_{DQP}}{\partial z_Q} = \gamma_{DQ} + \beta_{DQ}\frac{\partial y_Q}{\partial z_Q} + \gamma_{PQ} + \beta_{PQ}\frac{\partial y_Q}{\partial z_Q}. \quad (5)$$

By combining Eqs. (2)–(5), the expressions for the meridional and sagittal components of the groove density at point $P$ can be obtained:

$$\frac{\partial n}{\partial x_P} = \frac{1}{\lambda}\left[\left(\alpha_{CP} + \beta_{CP}\frac{\partial y_P}{\partial x_P}\right) - \left(\alpha_{QP} + \beta_{QP}\frac{\partial y_P}{\partial x_P}\right)\right], \quad (6)$$

$$\frac{\partial n}{\partial z_P} = \frac{1}{\lambda}\left[\left(\gamma_{CP} + \beta_{CP}\frac{\partial y_P}{\partial z_P}\right) - \left(\gamma_{QP} + \beta_{QP}\frac{\partial y_P}{\partial z_P}\right)\right]. \quad (7)$$

Based on the deduction above, and assuming that the recording structure parameters ($L_{RC}$, $L_{RQ}$, $L_{RD}$, $\theta_C$, $\theta_Q$) have been selected, the recording structure design can be converted into a calculation of the description of the reflective mirror from the known groove distribution coefficients. The parameter $\theta_D$ is ignored in this case because it can be decided using Eq. (7) along with the definition of the groove density at the center of the grating and $\theta_C$. The complete design strategy is introduced as follows (see Fig. 2):

(1) obtain the optical path $L_{CP_i} - L_{CO}$ and the directional vectors $\alpha_{CP_i}$, $\beta_{CP_i}$, and $\gamma_{CP_i}$ for each of the sampling points $P_i$ on the grating substrate;
(2) the relative optical path difference $L_{DQ_iP_i} - L_{DO_1O}$ and directional vectors $\alpha_{Q_iP_i}$, $\beta_{Q_iP_i}$, and $\gamma_{Q_iP_i}$ of sampling point $P_i$ in the aspherical wavefront recording beam can then be determined using Eqs. (1), (6), and (7);

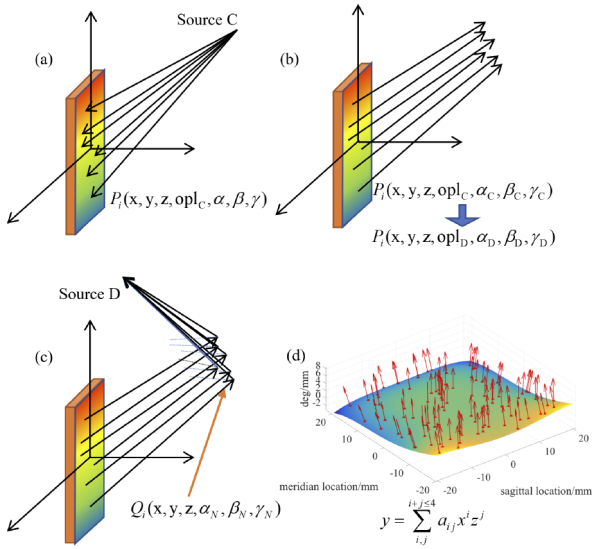


**Fig. 2.** Reconstruction process for a single structure: (a) calculation of the optical path and the direction of incidence in the spherical beam at feature point $P_i$; (b) calculation of the optical path difference and the direction of incidence in the aspherical beam at each feature point $P_i$; (c) calculation of the coordinates and the normal direction of $Q_i$ based on the optical path definition; (d) surface fitting performed to obtain the description of the auxiliary mirror.

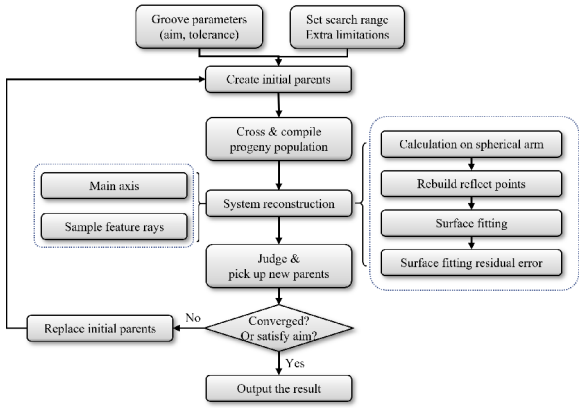


**Fig. 3.** Flow chart of the design process.

(3) by combining the known $L_{RD}$, $L_{RQ}$, $\theta_D$, and $\theta_Q$ with the optical path difference $L_{DQ_iP_i} - L_{DO_1O}$ and the directional vectors $\alpha_{Q_iP_i}$, $\beta_{Q_iP_i}$, and $\gamma_{Q_iP_i}$ obtained in step 2, it is possible to solve for the coordinates of the corresponding reflection point $Q_i$ on the auxiliary mirror for each sample point $P_i$, and the corresponding surface normal information at $Q_i$ can be obtained simultaneously;

(4) a fitting method for the coordinates and the normal information of feature point $Q_i$ obtained in step 3 is then used to obtain the surface description [8,17] and complete the entire recording structure design.

Therefore, the optimization matter for design of the recording structure can be converted from determination of the groove distribution coefficients to determination of the mirror fitting matter using this reconstruction method, which means that the multi-objective matter and the expansion residual error of the groove distribution coefficients can be avoided. However, it is also necessary to optimize the recording structure parameters using an optimization algorithm to achieve the best possible ground shape fitting, i.e., to reduce the residual surface shape fitting error. In addition, a specific tolerance error is allowed for the groove distribution in most cases. In this reconstruction design method, the groove distribution coefficients can also be used as part of the optimization parameters. By selecting the coefficients to be within the allowable tolerances and the recording structure parameters of the recording structure for use as the optimization parameters, the program takes the peak-to-valley value or the root mean square value of the residual surface fitting error as the single evaluation objective. Finally, with the aid of a genetic algorithm, a complete optimization process for design of the VLS grating recording system is established. Figure 3 shows the flow chart for the complete design process.

A planar VLS grating for use in a synchrotron radiation source beamline station is designed to demonstrate the accuracy of the proposed reconstruction method. The grating is required to have a specified groove distribution within an area of $210 \times 30\text{mm}^2$ on the plane, and the equivalent groove density at the grating center is 1200 g/mm. The groove distribution on the meridian plane is designed using both the expansion method and the reconstruction method. The absolute error and relative error distributions of the groove density obtained using these two design methods are shown in Fig. 4. Because of the influence of the higher-order terms that were ignored in the expansion method, there is an inherent error in the groove density between the

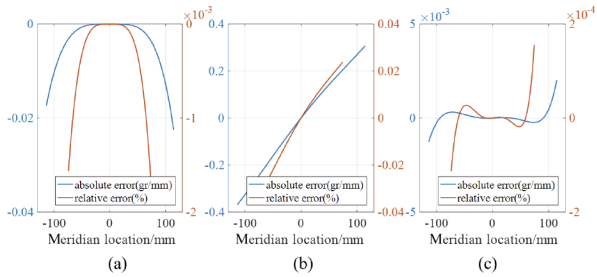


**Fig. 4.** (a) Absolute error and relative difference in the groove density between the designed value and the ray-tracing value obtained based on the expansion method. (b) Absolute error and relative error distributions of the groove density between the designed result and the intended design obtained by using the expansion method. (c) Absolute error and relative error distributions for the groove density between the design result and the intended design obtained by using the reconstruction method.

design result and the ray-tracing-based result, and the maximum error is 0.023 g/mm. The maximum value of this groove density error between the design result and the intended design obtained via the expansion method is 0.36 g/mm within the full range of the grating meridian diameter. The results obtained by using the reconstruction design method show greater accuracy, and the maximum density error is reduced to 0.002 g/mm. Although both the traditional method and the reconstruction method can obtain groove distributions that meet the design requirements, the reconstruction method achieves greater accuracy.

Because this VLS grating is designed to be within a $210 \times 30\text{mm}^2$ aperture size, a full-size design is required. Therefore, we conducted additional design tests for the groove distribution at the full grating size. The spherical surface was still used as the fitting target for the auxiliary mirror in this case, and all optimization control parameters remained unchanged. Because the grating was designed to have varied line-space and straight lines, control of the sag distribution of the groove within the design process leads to out-of-control results. The error in the groove function ranges up to $336\lambda$. The sagittal and meridional components of the groove density error reached maxima of 3.38 g/mm and 8.76 g/mm, with averages of 0.75 g/mm and 2.84 g/mm, respectively. We converted the surface fitting target of the auxiliary mirror from a spherical surface into a freeform surface, which can be described as a polynomial with a specific order. With all control parameters remaining constant, the final design result was obtained after ten iterations. Over the entire grating aperture, the groove function error was less than $0.14\lambda$, and the sagittal and meridional components of the groove density error were less than 0.01 g/mm and 0.005 g/mm, respectively. Figure 5 shows a comparison between these two design results within the normalized grating aperture, including the groove function error, and the meridional and sagittal components of the groove density error. The horizontal axis represents the normalized meridian coordinate of the VLS grating, and the vertical axis represents its normalized sagittal coordinate. In addition, parallel calculations were used to perform simultaneous fitting of the feature points of each offspring individual, which greatly reduced the extra time required when compared with the traditional circle method. This comparison result shows that the numerous design degrees of freedom of freeform surfaces offer an enhanced capability for realization of VLS grating designs.

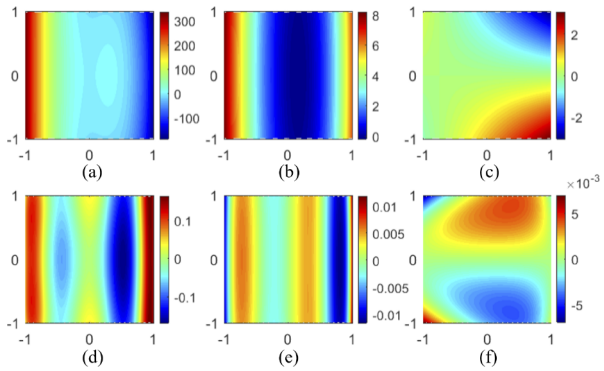


**Fig. 5.** Comparison of the groove distributions of the spherical mirror added system and the freeform mirror added system: (a) optical distance error characteristics for the spherical mirror added system; (b) meridional density error characteristics for the spherical mirror added system; (c) sagittal density error characteristics for the spherical mirror added system; (d) optical distance error characteristics for the freeform mirror added system; (e) meridional density error characteristics for the freeform mirror added system; (f) sagittal density error characteristics for the freeform mirror added system

In this Letter, a reconstruction design method for an aspherical recording system is proposed for VLS gratings. The recording system design is converted into a reconstruction of the surface shape of the auxiliary mirror from a known groove distribution by searching for a suitable recording structure parameters. Genetic algorithms are used to realize global optimization. The results of the forward ray-tracing approach used here effectively verify that this reconstruction design method achieves greater design accuracy than the traditional expansion method. By replacing the auxiliary mirror fitting target with other mirror types, including ellipsoid meridians, parabolic mirrors, and freeform mirrors, this method can be extended to optimal design of aspherical recording systems for arbitrary VLS gratings. The numerous design degrees of freedom of freeform surfaces offer great advantages for realization of specific groove distributions.

**Funding.** National Key Research and Development Program of China (2020YFA0714500); Scientific Instruments and Equipments Development Project of the Chinese Academy of Science (YJKYYQ20200003); National Natural Science Foundation of China (12105288, 61905244); The Program for the Development of Science and Technology Jilin Province (20200801055GH).

**Disclosures.** The authors declare no conflicts of interest.

**Data availability.** Data underlying the results presented in this paper are not publicly available at this time but may be obtained from the authors upon reasonable request.

## REFERENCES

1. G. Ghiringhelli, A. Piazzalunga, C. Dallera, G. Trezzi, L. Braicovich, T. Schmitt, V. N. Strocov, R. Betemps, L. Patthey, and X. Wang, Rev. Sci. Instrum. **77**, 113108 (2006).
2. Y. Harada, M. Kobayashi, H. Niwa, Y. Senba, H. Ohashi, T. Tokushima, Y. Horikawa, S. Shin, and M. Oshima, Rev. Sci. Instrum. **83**, 013116 (2012).
3. Z. Yin, H. B. Peters, U. Hahn, M. AgåKer, A. Hage, R. Reininger, F. Siewert, J. Nordgren, J. Viefhaus, and S. Techert, Rev. Sci. Instrum. **86**, 093109 (2015).
4. A. Shatokhin, A. Kolesnikov, P. Sasorov, E. Vishnyakov, and E. Ragozin, Opt. Express **26**, 19009 (2018).
5. E. A. Vishnyakov, A. O. Kolesnikov, A. N. Shatokhin, and E. N. Ragozin, Proc. SPIE **10677**, 106770E (2018).
6. E. R. Muslimov, M. Ferrari, E. Hugot, J.-C. Bouret, C. Neiner, S. Lombardo, G. R. Lemaitre, R. Grange, and I. A. Guskov, Opt. Eng. **57**, 12510 (2018).
7. E. N. Ragozin, A. O. Kolesnikov, A. S. Pirozhkov, P. V. Sasorov, and E. A. Vishnyakov, in *X-Ray Lasers 2018. ICXRL 2018*, Vol. 241 of Springer Proceedings in Physics (Springer, 2018).
8. B. Zhang, Y. Tan, J. Zhu, and G. Jin, Opt. Lett. **46**, 3412 (2021).
9. Y. Shimizu, R. Ishizuka, K. Mano, Y. Kanda, and W. Gao, Precis. Eng. **67**, 36 (2021).
10. X. Yang and T.-C. Weng, Rev. Sci. Instrum. **92**, 123104 (2021).
11. T. Namioka and M. Koike, Appl. Opt. **34**, 2180 (1995).
12. M. Duban, Appl. Opt. **38**, 1096 (1999).
13. L. Qing, W. Gang, L. Bin, and W. Qiuping, Appl. Opt. **45**, 5059 (2006).
14. X. Chen and L. Zeng, Appl. Opt. **57**, 7281 (2018).
15. X. Chen and L. Zeng, Opt. Express **27**, 3294 (2019).
16. J. P. Rolland, M. A. Davies, T. J. Suleski, C. Evans, A. Bauer, J. C. Lambropoulos, and K. Falaggis, Optica **8**, 161 (2021).
17. Y. Tong, G. F. Jin, and J. Zhu, Light: Sci. Appl. **6**, e17081 (2017).